INTERNATIONAL JOURNAL OF RESEARCH AND INNOVATION IN APPLIED SCIENCE (IJRIAS)
ISSN No. 2454-6194 | DOI: 10.51584/IJRIAS |Volume XI Issue XIII July 2026
Special Issue on Innovations in Environmental Science and Sustainable Engineering

Integrated Structural and Foundation Performance Assessment of an SST-3L-52M-LIGHT Telecommunication Tower

Dyna Prasetya Riani[1]*, Aep Saepuloh[2], Ade Suhendar S.[3], Nurina Yasin[4]

[1,4]Master of Civil Engineering Study Program, Gunadarma University, Jakarta, Indonesia

[2,3]Master of Civil Engineering Study Program, Universitas Nusa Megarkencana, Daerah Istimewa Yogyakarta, Indonesia

***Corresponding Author**

DOI: https://doi.org/10.51584/IJRIAS.2026.11013SP0028

Received: 15 July 2026; Accepted: 20 July 2026; Published: 30 July 2026

ABSTRACT

Communication towers are slender infrastructure systems whose safety depends on the interaction of the steel lattice superstructure, connections, anchorage, and foundation. This study presents an integrated case evaluation of a 52 m three-legged self-supporting telecommunication tower (SST-3L-52M-LIGHT) located at the Tanjung Priok Access Toll Road Operational Office, North Jakarta. The structural model was evaluated in SAP2000 using SNI 1727:2020, SNI 1726:2019, and SNI 1729:2020. The assessment covered dead, live, and directional wind loads; compression-member capacity; bolted connections; base-plate and anchor-bolt resistance; and bored-pile capacity under compression and uplift, including a flood condition represented by a reduced effective concrete unit weight. To extend the single-case evaluation, directional comparison and wind-demand sensitivity analyses were conducted using three basic wind-speed scenarios while retaining the original geometry and aerodynamic coefficients. The y-direction wind demand was 56.69 kN, 15.46% higher than the x-direction demand of 49.10 kN, and the gravity-plus-y-wind combination (COMB4) governed the design. The critical L150×150×15 leg member carried 287.50 kN against a design compressive resistance of 652.71 kN, giving a utilization ratio of 0.44. The bolt group, base plate, and anchor system also satisfied their respective resistance checks. Under the flood-adjusted condition, the bored-pile system provided 422.44 kN compression resistance against 376.81 kN demand and 341.17 kN uplift resistance against 267.76 kN demand. Wind-demand scaling increased the equivalent y-direction load to 106.58 kN and 172.85 kN for basic wind speeds of 45.70 and 58.20 m/s, respectively. The study contributes a traceable superstructure-to-foundation assessment under a consistent Indonesian code framework, while explicitly limiting its conclusions to the evaluated geometry, loading assumptions, and geotechnical data.

Keywords: telecommunication tower; steel lattice structure; wind-load sensitivity; connection design; bored-pile foundation

INTRODUCTION

Telecommunication lattice towers support antennas and ancillary equipment whose continued operation is critical to wireless communication networks. Their low mass, high slenderness, limited inherent damping, and large exposed area make wind a dominant action, although the adequacy of the complete system also depends on connection detailing, anchorage, and foundation response. Recent lattice-tower research has shown that wind loading cannot be represented solely as a single static pressure problem. Dynamic force reconstruction and spectral simulation studies have demonstrated that structural response is influenced by modal properties, spatial coherence, and skew-wind effects (Zhang et al., 2023a; Zhang et al., 2023b). Aeroelastic testing has also indicated that code-based drag coefficients and gust response factors may underestimate demand for some lattice configurations (Jeddi et al., 2023). These findings do not invalidate code-based design, but they show that deterministic equivalent-static analysis should be interpreted as a bounded engineering model rather than a complete representation of wind–structure interaction.

A second development in the 2023–2026 literature is the increasing use of monitoring and probabilistic assessment. Saleem et al. (2023) used vibration features and machine-learning techniques for communication-tower health monitoring, demonstrating the potential of operational data for detecting changes that cannot be inferred from a one-time design check. Kenéz and Joó (2024) combined a finite-element model, site measurements, Bayesian extreme-wind estimation, and performance-based assessment for a telecommunication lattice mast. Their work is methodologically stronger than a conventional deterministic check because it represents uncertainty in wind and structural parameters; however, it also requires monitoring data and probabilistic expertise that are not routinely available for many tower projects. Full-scale monitoring by Calotescu et al. (2025) further showed that synoptic and thunderstorm winds produce distinguishable response patterns in a 50 m telecommunication lattice tower. Consequently, a design based only on a basic wind-speed value may not fully describe non-synoptic events, particularly when transient gust structure differs from the assumptions embedded in standard exposure models.

Long-term measurements have also challenged the assumption that tower dynamic properties are constant. Mengistu et al. (2026) reported environmentally dependent natural frequencies and wind-dependent aerodynamic damping in a 50 m self-supporting lattice tower; the damping ratios of the first modes increased substantially with mean wind speed. This observation is important because fixed damping values are commonly adopted in analytical models. Nevertheless, monitoring results are site- and structure-specific and should be used to calibrate, rather than automatically replace, code-based models. At a lower computational cost, Moussavi et al. (2025) demonstrated that tapering geometry affects the dynamic response of telecommunication towers and proposed a homogenized analytical model. Their results reinforce the need to treat geometry as an active response parameter rather than assuming transferability between towers of equal height.

Wind directionality is another recurrent issue. Zhu et al. (2024) used nonlinear fragility analysis for a transmission tower and found that the most unfavorable attack angle was not necessarily aligned with a principal axis. Large-scale aeroelastic tests by Mazaheri and Alipour (2026) similarly showed that skewed wind and aerodynamic interaction can materially alter measured forces. These transmission-tower studies are not directly equivalent to an isolated BTS tower because conductors and multispan coupling introduce additional dynamics. They are nevertheless relevant as methodological evidence that checking only two orthogonal wind directions may miss an adverse oblique direction. The present study therefore treats its x–y comparison as a directional screening exercise, not as proof that all wind attack angles have been enveloped.

Recent case studies in Indonesia and other developing-country settings remain predominantly deterministic. Cahyono et al. (2024) assessed a BTS upper structure and its joint components in a high-wind region, whereas Marsia and Siregar (2024) showed that additional antenna loading could increase the stress ratio of a 72 m SST tower beyond the allowable limit. Romero Romero et al. (2025) used cross-software verification for a 36 m self-supporting tower and identified secondary-bracing slenderness deficiencies despite acceptable global seismic indicators. Collectively, these studies demonstrate that global stability alone is insufficient; equipment changes and secondary members may control safety. However, they primarily concentrate on the upper structure and do not trace the design load path through the anchorage into a site-specific bored-pile foundation.

Steel-system selection in developing regions is additionally conditioned by fabrication accuracy, logistics, skilled-labour availability, cost, and access to specialist support. Fahim et al. (2026) documented the implementation of light-gauge and hot-rolled steel systems in the seismically active and resource-constrained context of Badakhshan Province, Afghanistan. The structural typology differs from a telecommunication lattice tower, so the study cannot be used as direct evidence for tower capacity. Its relevance is contextual: a technically adequate steel system may still be unsuitable if fabrication, quality control, transport, or local implementation capacity is not addressed.

Against this background, the principal research gap is not the absence of another finite-element calculation, but the limited integration of recent wind-response knowledge with a complete, project-level load path from lattice members to bored-pile foundation. This study evaluates the SST-3L-52M-LIGHT tower at Tanjung Priok using SNI 1727:2020, SNI 1729:2020, and SNI 1726:2019 (Badan Standardisasi Nasional, 2020a, 2020b, 2019). Its contribution is threefold: (1) an integrated assessment of the superstructure, connection system, anchorage, and bored-pile foundation; (2) an explicit comparison of wind demand in the two principal directions; and (3) a basic wind-speed sensitivity assessment that exposes the boundary of a single-site adequacy conclusion. The study does not claim a new finite-element or probabilistic method. Its contribution is an auditable engineering integration that is directly applicable to project review while remaining transparent about the limitations of deterministic analysis.

Theoretical And Design Basis

Load model and combinations

The tower was evaluated for structural self-weight, additional dead load from antenna equipment, worker/equipment live load, and wind load. SAP2000 automatically calculated the steel self-weight; a multiplier of 1.05 was applied to account for bolts and connection plates. The load combinations used in the original design evaluation were:

- COMB1 = 1.4D + L
- COMB2 = 1.2D + 1.6L
- COMB3 = 1.2D + L + $1.0W_x$
- COMB4 = 1.2D + L + $1.0W_\gamma$
- COMB5 = 0.9D + $1.0W_x$
- COMB6 = 0.9D + $1.0W_\gamma$

The equivalent static wind force applied to a tower panel was calculated as:

$F = q_z G C_f A_f$	(1)
$q_z = 0.613 k_z k_{zt} k_d k_e V^2$	(2)
$C_f = 3.4\varepsilon^2 - 4.7\varepsilon + 3.4$	(3)
$A_f = \varepsilon A_g$	(4)

where q_z is the velocity pressure (N/m²), k_z is the exposure coefficient, k_{zt} is the topographic factor, k_d is the directionality factor, k_e is the elevation factor, V is the basic wind speed (m/s), G is the gust factor, C_f is the force coefficient, ε is the solidity ratio, A_g is the gross projected area, and A_f is the effective projected area. The case calculation adopted $k_z = 1.23$, $k_{zt} = 1.00$, $k_d = 0.85$, $k_e = 1.00$, G = 0.85, ε = 0.25, and V = 33.33 m/s, consistent with the original calculation sheet.

Table 1. Wind-speed scenarios used for the demand-sensitivity assessment

Scenario	**Basic wind speed V (m/s)**	**Relative pressure V^2/V_1^2**
S1 – site design case	33.33	1.000
S2 – intermediate wind case	45.70	1.880
S3 – high wind case	58.20	3.049

ISSN No. 2454-6194 | DOI: 10.51584/IJRIAS |Volume XI Issue XIII July 2026
Special Issue on Innovations in Environmental Science and Sustainable Engineering

Compression-member resistance

Angle-section leg and bracing members were checked for local slenderness and flexural buckling in accordance with SNI 1729:2020 (Badan Standardisasi Nasional, 2020b). For a compression member, the elastic buckling stress, critical stress, nominal resistance, and design resistance were calculated as follows:

$F_e = \pi^2 E / (L_c/r)^2$	(5)
$F_{cr} = 0.658^{(F_y/F_e)} F_y \text{ for } L_c/r \leq 4.71\sqrt{(E/F_y)}$	(6)
$F_{cr} = 0.877 F_e \text{ for } L_c/r > 4.71\sqrt{(E/F_y)}$	(7)
$P_n = F_{cr} A_g$	(8)
$P_u / (\varphi_c P_n) \leq 1.0$	(9)

The original evaluation used a project acceptance threshold of 0.95 for the reported utilization ratio, providing a small margin below the nominal LRFD limit of 1.0.

Connections, base plate, and anchors

The bolt group was checked against the factored axial force transferred by the critical leg. The base plate was evaluated for concrete bearing and cantilever bending, while anchor bolts were checked for combined tension and shear. The principal expressions were:

$\varphi R_n = \varphi F_{nv} A_b n$	(10)
$A_{b,min} = P_u / (0.5 \times 0.85 f'_c)$	(11)
$f_b = P_u / B^2$	(12)
$M_u = 0.5 f_b B a^2$	(13)
$f_{bend} = M_u / Z \leq \varphi F_y$	(14)

where A_b is the bolt shear area, n is the number of bolts, B is the plate width, a is the plate projection beyond the angle leg, and Z is the plastic section modulus of the plate strip.

Bored-pile capacity and uplift stability

Pile resistance was calculated from cone penetration test (CPT) data using the Meyerhof approach (Meyerhof, 1976), supported by the foundation-design procedures summarized by Hardiyatmo (2018). The expressions retained from the original design calculation were:

$A_p = \pi D^2/4$	(15)
$W_p = A_p L \gamma_c$	(16)
$Q_{fr} = (\pi D L T_f)/SF_2$	(17)
$Q_e = (A_p q_c)/SF_1$	(18)
$Q_t = Q_{fr} + Q_e - W_p$	(19)
$Q_n = n Q_t$	(20)

INTERNATIONAL JOURNAL OF RESEARCH AND INNOVATION IN APPLIED SCIENCE (IJRIAS)
ISSN No. 2454-6194 | DOI: 10.51584/IJRIAS |Volume XI Issue XIII July 2026
Special Issue on Innovations in Environmental Science and Sustainable Engineering

$$Q_{tr} = n(0.75Q_{fr}) + W_p \quad (21)$$

Compression and uplift stability were verified by comparing the applicable group capacities with the maximum factored support reactions. For the flood case, the effective unit weight of submerged concrete was reduced to 14 kN/m³, thereby lowering the stabilizing foundation weight.

METHOD

Case-study object and data sources

The evaluated structure is a 52 m high three-legged self-supporting lattice tower located at the Tanjung Priok Access Toll Road Operational Office, North Jakarta. The tower has a triangular plan, a base width of 4.804 m, angle-section steel legs and bracing, reinforced-concrete pedestals and pile caps, and four 0.40 m diameter bored piles per tower leg. The principal input data were obtained from the as-planned drawings, project load schedule, SAP2000 model, and site CPT record.

Table 2. Principal tower and foundation characteristics

Parameter	**Value**
Tower type	Three-legged self-supporting lattice tower
Tower model	SST-3L-52M-LIGHT
Height	52 m
Base width	4.804 m
Plan shape	Equilateral triangular
Main structural sections	Steel angle sections
Foundation	Four bored piles per leg, diameter 0.40 m
Pile cap	Reinforced-concrete pile cap
Pedestal	Reinforced-concrete column

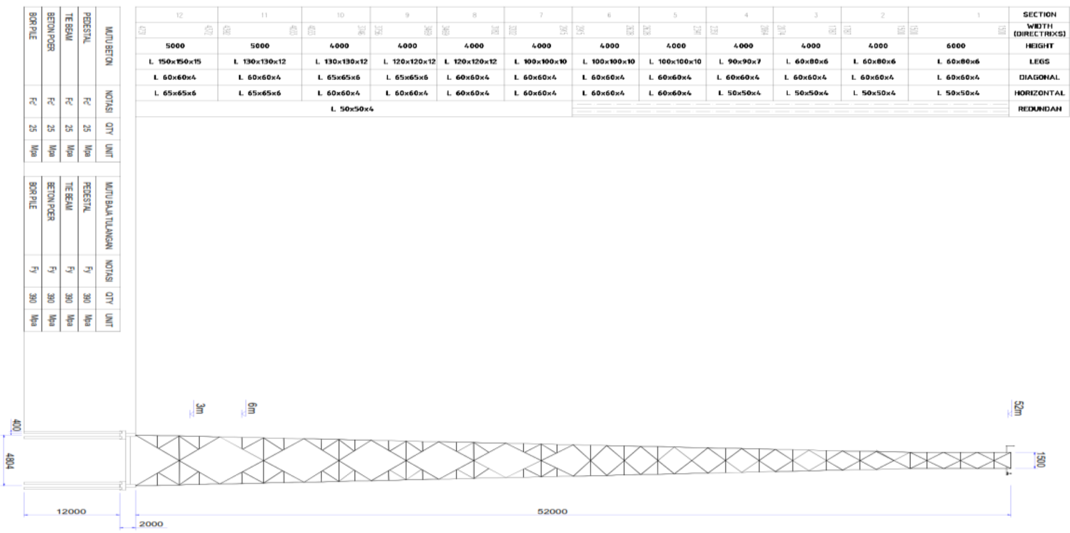

Figure 1. Tower elevation, geometry, and member schedule from the project drawing.

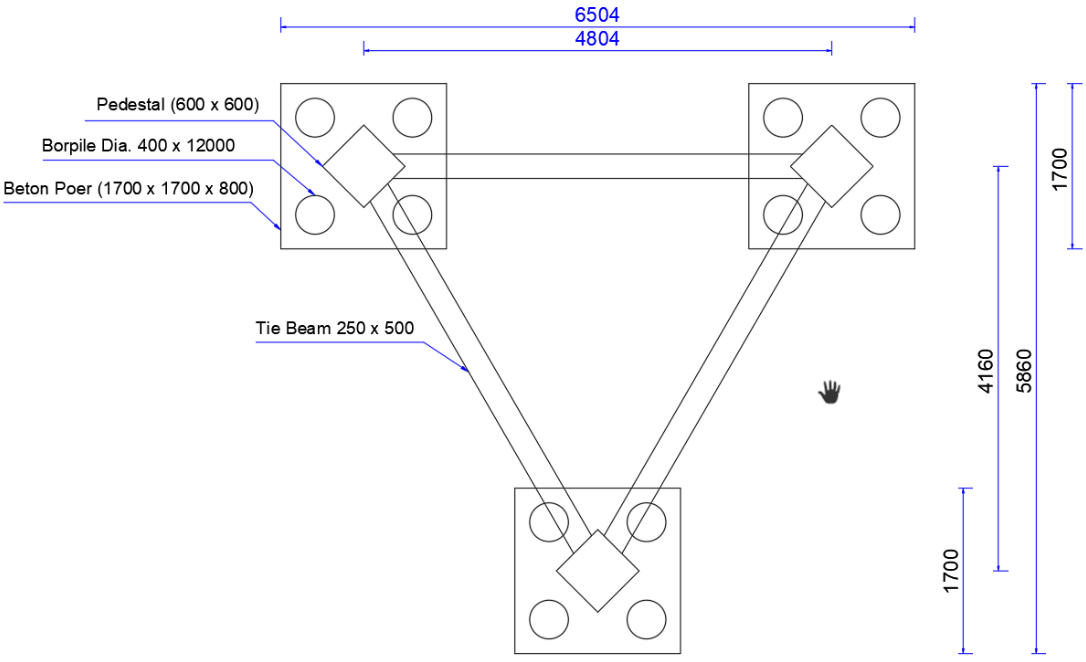

Figure 2. Plan layout of the three foundation groups.

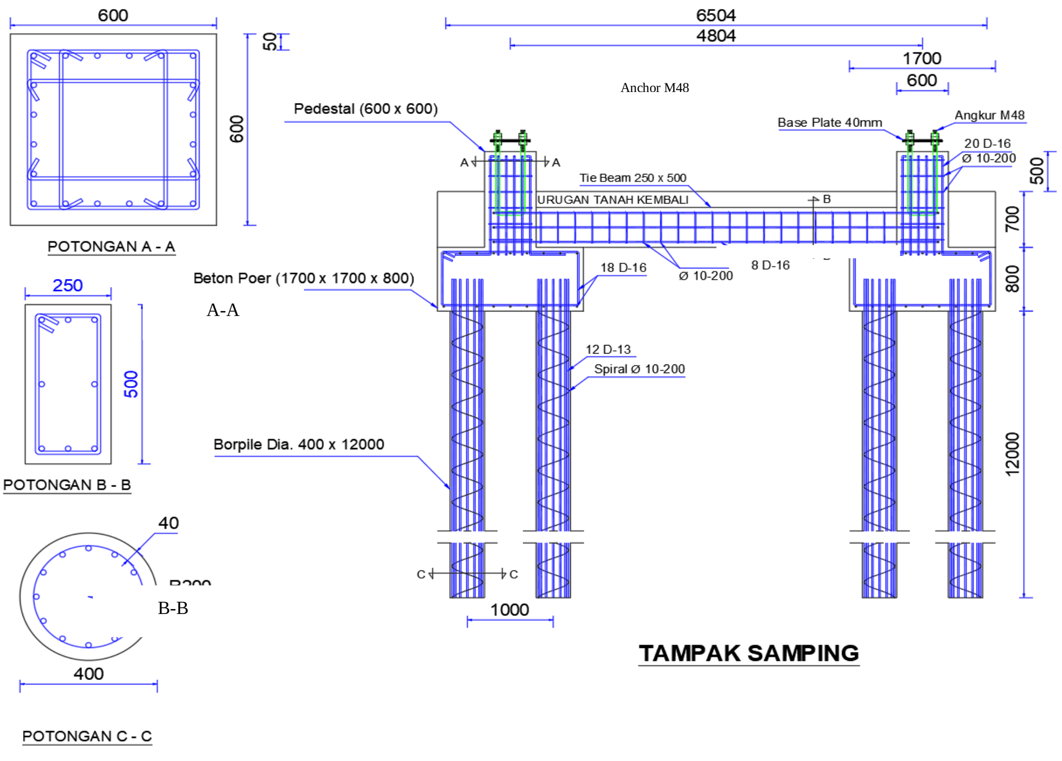

Figure 3. Foundation and bored-pile reinforcement details.

Numerical modeling and evaluation sequence

The tower was modeled as a three-dimensional lattice frame in SAP2000. Steel angle members were represented as frame elements connected at the tower joints. Dead and live loads were applied at the specified elevations, and equivalent nodal wind forces were distributed to the three main nodes at each panel level. The evaluation sequence comprised load definition, model analysis, identification of the governing combination, member-capacity checks, connection and anchorage checks, and foundation-capacity checks. Figure 4 summarizes this sequence.

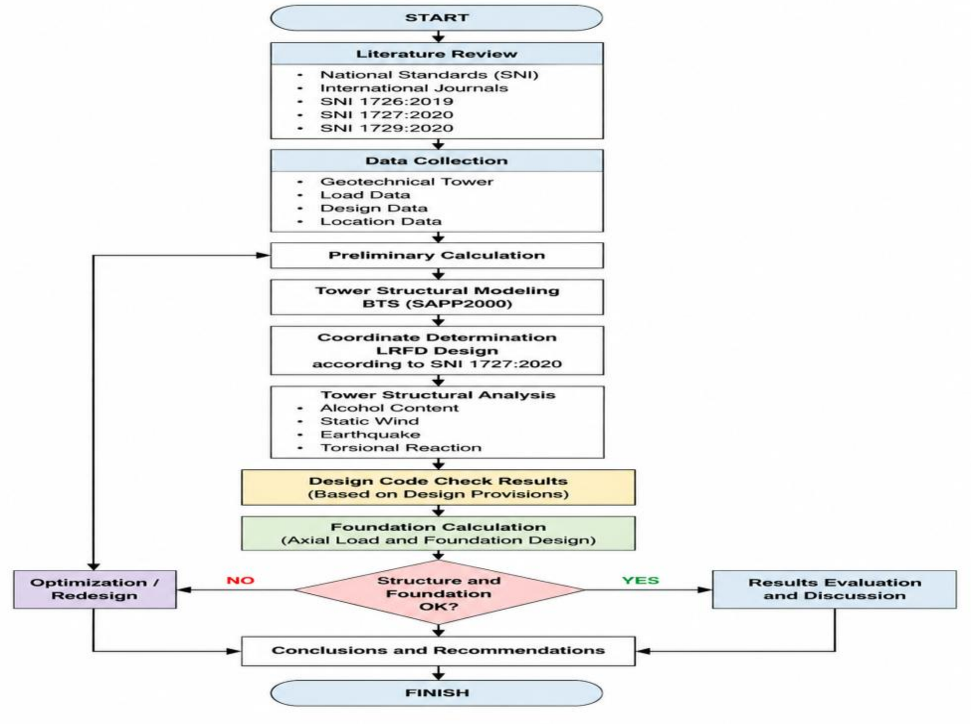

Figure 4. Structural and foundation evaluation workflow.

Applied gravity and equipment loads

The antenna dead load consisted of three 0.25 kN point loads at elevation 47.00 m and three 0.25 kN point loads at elevation 49.00 m. The live load representing a worker and equipment was 1.10 kN at each of the two service elevations, distributed to the designated main nodes. The self-weight multiplier for the DEAD load case was 1.05.

Wind-demand sensitivity procedure

To address the limited transferability of a single design case, the equivalent wind demand was re-evaluated for the three basic wind-speed scenarios in Table 1. Geometry, solidity, directionality, exposure, topography, and gust factors were held constant. Because velocity pressure is proportional to V^2, the total x- and y-direction loads were scaled by $(V_i/V_1)^2$. This procedure is deliberately framed as a demand-level sensitivity analysis. It isolates the first-order influence of wind-speed variation, but it does not reproduce changes in modal response, aerodynamic damping, oblique-wind loading, non-synoptic gust structure, or nonlinear redistribution. Complete member utilization and foundation reactions for Scenarios S2 and S3 would require rerunning the SAP2000 model and, for high-fidelity assessment, calibrating the aerodynamic assumptions against monitoring or wind-tunnel evidence (Kenéz and Joó, 2024; Calotescu et al., 2025; Mengistu et al., 2026).

Geotechnical data

CPT sounding was performed with a 2.5-ton apparatus equipped with a Begemann adhesion-jacket cone. The test was continued to the hard layer, where cone resistance reached approximately 250 kg/cm². Selected readings used in the foundation evaluation are presented in Table 3.

Table 3. Selected CPT results at the SST-3L-52M-LIGHT site

Depth (m)	Cone resistance q_c (kg/cm²)	Cumulative friction T_f (kg/cm)
1	6	18.71

2	10	36.08
3	48	70.83
9	5	248.58
10	10	281.99
11	10	322.08
12	12	355.50
13	18	435.68
14	39	498.49
15	43	569.33
16	85	646.84
17	90	709.65
18	250	775.14

RESULTS AND DISCUSSION

Directional wind demand

For the design wind speed of 33.33 m/s, the adopted coefficients produced q_z = 710.68 N/m² and C_f = 2.44. The effective projected areas were 38.50 m² in the y direction and 33.34 m² in the x direction. The resulting total equivalent nodal loads were 56.69 kN and 49.10 kN, respectively. Thus, the y-direction demand exceeded the x-direction demand by 7.59 kN, or 15.46%, explaining why COMB4 (gravity plus W_{γ}) governed the reported member checks. This result confirms that even a triangular tower does not necessarily present equal projected demand in its principal directions. It must not, however, be interpreted as a complete directional envelope: nonlinear fragility analysis and aeroelastic testing of related lattice systems have shown that oblique wind can produce more adverse response than orthogonal wind (Zhu et al., 2024; Mazaheri and Alipour, 2026).

$F_y = 710.68 \times 0.85 \times 2.44 \times 38.50 = 56.69\ kN$	(22)
$F_x = 710.68 \times 0.85 \times 2.44 \times 33.34 = 49.10\ kN$	(23)

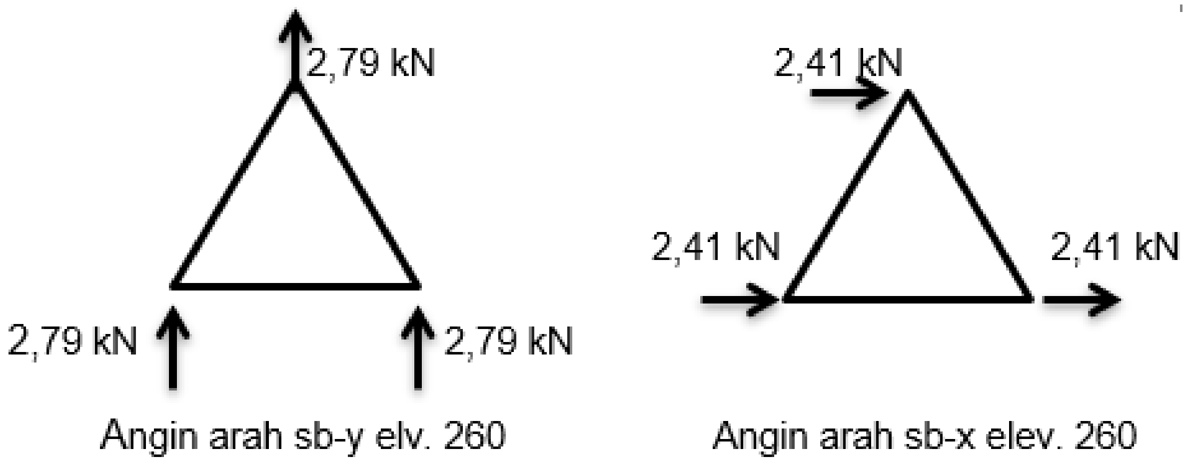

Figure 5. Equivalent nodal wind loading at the lowest analyzed elevation.

Table 4. Distribution of y-direction wind force

Elevation (cm)	Projected area (m^2)	F_y (kN)	F_y per node (kN)
260	23.12	8.36	2.79
760	21.28	7.69	2.56
1210	15.77	5.70	1.90
1610	14.62	5.28	1.76
2010	13.47	4.87	1.62
2410	12.32	4.45	1.48
2705	8.67	3.13	1.04
2905	5.44	1.97	0.66
3105	5.15	1.86	0.62
3305	4.87	1.76	0.59
3505	4.58	1.66	0.55
3705	4.29	1.55	0.52
3905	4.01	1.45	0.48
4105	3.72	1.34	0.45
4305	3.43	1.24	0.41
4505	3.14	1.13	0.38
4700	3.00	1.08	0.36
4900	3.00	1.08	0.36
5100	3.00	1.08	0.36
Total	156.90	56.69	—

Table 5. Distribution of x-direction wind force

Elevation (cm)	Projected area (m^2)	F_x (kN)	F_x per node (kN)
260	20.02	7.24	2.41
760	18.43	6.66	2.22
1210	13.66	4.94	1.65

1610	12.66	4.58	1.53
2010	11.67	4.22	1.41
2410	10.67	3.86	1.29
2705	7.51	2.71	0.90
2905	4.71	1.70	0.57
3105	4.46	1.61	0.54
3305	4.22	1.52	0.51
3505	3.97	1.43	0.48
3705	3.72	1.34	0.45
3905	3.47	1.25	0.42
4105	3.22	1.16	0.39
4305	2.97	1.07	0.36
4505	2.72	0.98	0.33
4700	2.60	0.94	0.31
4900	2.60	0.94	0.31
5100	2.60	0.94	0.31
Total	135.90	49.10	—

Wind-speed sensitivity

Table 6 quantifies the effect of wind-speed variation while retaining the project geometry and coefficients. Increasing V from 33.33 to 45.70 m/s increased velocity pressure and total equivalent wind demand by a factor of 1.88. At 58.20 m/s, the demand factor was 3.049. This quadratic escalation is structurally significant: a tower that satisfies a low-wind site cannot be assumed adequate at another site solely because its geometry and equipment loading are unchanged. The finding is consistent with performance-based research showing that the wind-hazard model is a primary contributor to response uncertainty (Kenéz and Joó, 2024). At the same time, simple V^2 scaling retains the original force and gust coefficients. Because aeroelastic evidence suggests that these coefficients can be configuration-dependent and, in some cases, underestimated by standard formulations, the scaled values should be treated as screening demands rather than final design actions (Jeddi et al., 2023).

Table 6. Parametric sensitivity of equivalent wind demand

Scenario	**V (m/s)**	**Scale factor**	**F_x (kN)**	**F_y (kN)**	**Change in F_y from S1**
S1	33.33	1.000	49.10	56.69	—
S2	45.70	1.880	92.31	106.58	+88.0%

S3	58.20	3.049	149.71	172.85	+204.9%

The sensitivity results provide a transparent but limited form of parametric variation that was absent from the initial manuscript. Their value is diagnostic: they quantify how quickly the external demand changes and identify when a full reanalysis becomes necessary. They do not establish structural adequacy for Scenarios S2 and S3 because load redistribution, second-order effects, member buckling, connection force, and foundation reaction must be obtained from the structural model. They also do not simulate thunderstorm outflows, whose transient characteristics and tower responses may differ from those associated with synoptic winds (Calotescu et al., 2025).

Structural member performance

The SAP2000 results identified COMB4 as the governing load combination for the reported compression members. Figure 6 shows the analytical tower model. The highest utilization occurred in leg member 5862, an L150×150×15 section. Its factored compression was 287.50 kN and its design resistance was 652.71 kN, resulting in a utilization ratio of 0.44. All reported ratios were below the project threshold of 0.95.

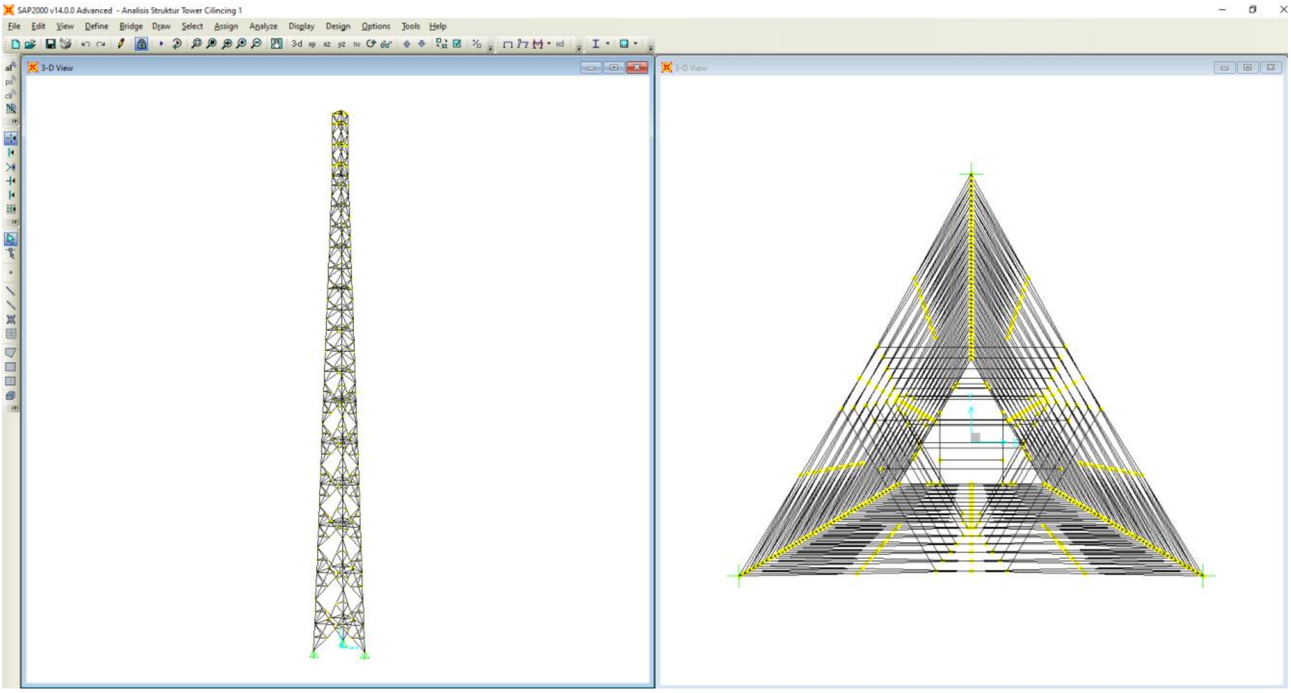

Figure 6. SAP2000 model of the tower in elevation and plan views.

Table 7. Compression-member design results under COMB4

Member	**Profile**	**Length (cm)**	**P_u (kN)**	**L_c/r**	**F_cr (MPa)**	**φP_n (kN)**	**Utilization**
5862	L150×150×15	130.00	287.50	82.53	169.64	652.71	0.44
6072	L130×130×12	105.00	200.03	80.92	171.93	460.48	0.43
6074	L130×130×12	95.10	198.81	78.95	174.71	467.94	0.42
6184	L120×120×12	105.00	163.17	82.74	169.34	416.98	0.39
6361	L100×100×10	105.00	106.60	87.29	162.79	278.38	0.38

6363	L100×100×10	95.01	105.68	84.69	166.54	284.78	0.37
6135	L70×70×7	145.30	21.31	113.94	123.88	103.80	0.21
6132	L70×70×7	135.50	24.96	110.30	129.14	108.20	0.23

The concentration of the largest demand in the lower main leg is mechanically consistent with the load path of a tapered lattice tower, where cumulative overturning action generates high axial force near the base. Nevertheless, recent case evidence shows that the member governing a code check is not always the visually dominant main leg. Marsia and Siregar (2024) found that additional antenna loading caused an unacceptable stress ratio until local strengthening was introduced, while Romero Romero et al. (2025) identified secondary-bracing slenderness deficiencies despite satisfactory global seismic indicators. The present utilization ratio of 0.44 therefore indicates reserve only for the reported model and member set; it does not exclude vulnerability arising from equipment modification, secondary members, connection eccentricity, corrosion, or fabrication imperfection.

Bolt group, base plate, and anchor system

The critical leg-to-base connection used fourteen A325 M20 bolts. The calculated bolt-group design shear resistance was 980.40 kN, exceeding the 311.13 kN factored leg force. For the 460 mm × 460 mm × 40 mm base plate, the minimum required bearing area was 29,283 mm², equivalent to a square side of 171.1 mm, which was smaller than the provided 460 mm width. The calculated bending stress was 44.14 MPa, below the design yield limit of 216 MPa. The anchor-bolt group resistance was 3,588.56 kN against a maximum tensile demand of 254.62 kN. These results confirm continuity of the load path from the steel leg to the pedestal for the evaluated design case.

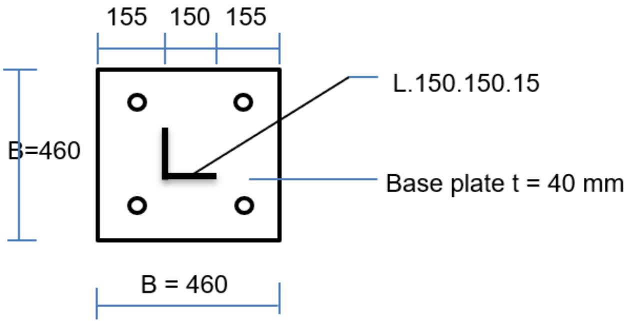

Figure 7. Base plate and critical leg arrangement.

Table 8. Summary of connection, base-plate, and anchorage checks

Component	**Demand**	**Resistance / limit**	**Demand-to-resistance conclusion**
A325 M20 bolt group	311.13 kN	980.40 kN	Satisfies
Base-plate bearing area	29,283 mm² required	211,600 mm² provided	Satisfies
Base-plate bending stress	44.14 MPa	216 MPa	Satisfies
Anchor-bolt tension group	254.62 kN	3,588.56 kN	Satisfies

Bored-pile and flood-adjusted foundation performance

For a 0.40 m diameter and 11.2 m long bored pile, the pile-tip area was 0.1256 m² (1,256 cm²) and the calculated pile self-weight was 19.69 kN. Using q_c = 12 kg/cm², cumulative friction T_f = 355.50 kg/cm, $SF_1 = 3$, and $SF_2 = 5$, the allowable shaft contribution was 89.30 kN, the tip contribution was 50.24 kN, and the net allowable compression capacity of one pile was 119.88 kN. The four-pile group therefore provided 479.50 kN in the direct pile-capacity check, exceeding the corresponding 376.48 kN compression demand. The direct uplift check produced 287.59 kN against 268.09 kN demand.

A second stability check considered the reduced effective concrete weight during flooding. The stabilizing weight was 54.522 kN, consisting of the steel frame contribution, pedestal column, pedestal block, and submerged pile-cap concrete. Combining this weight with the support reaction gave 376.81 kN maximum compression and 267.76 kN maximum uplift demand. The calculated flood-adjusted group resistances were 422.44 kN in compression and 341.17 kN in uplift. The corresponding reserves were 12.11% and 27.42%, respectively.

Table 9. Foundation capacity and stability summary

Foundation check	Demand (kN)	Resistance (kN)	Reserve	Status
Direct pile-group compression	376.48	479.50	27.4%	Satisfies
Direct pile-group uplift	268.09	287.59	7.3%	Satisfies
Flood-adjusted compression stability	376.81	422.44	12.1%	Satisfies
Flood-adjusted uplift stability	267.76	341.17	27.4%	Satisfies

The flood condition is relevant to the site context because buoyancy reduces the effective stabilizing weight. Explicitly including this condition extends the assessment beyond recent tower studies that are concentrated on aerodynamic response, monitoring, or upper-structure member checks. The resulting compression reserve of 12.11% is materially smaller than the 27.42% uplift reserve, indicating that the flood-adjusted compression condition is the more restrictive foundation check among those evaluated. This comparison also illustrates why a safe steel superstructure does not by itself establish system safety. Nevertheless, the foundation model remains static and does not represent scour, cyclic degradation, pile-group interaction nonlinearity, liquefaction, loss of soil confinement, or long-term deterioration; consequently, the calculated reserve should not be interpreted as a reliability index.

Comparison with recent studies and research contribution

Table 10. Critical positioning of the present study against selected literature published in 2023–2026

Study	Primary approach	Scope	Relationship to the present study
Zhang et al. (2023a; 2023b)	Generalized-force simulation and inverse reconstruction using aeroelastic data	Dynamic wind forces on steel lattice towers	Provides higher-fidelity wind-force representation; the present study uses equivalent-static demand and does not identify time-varying forces.
Jeddi et al. (2023)	Aeroelastic wind-tunnel testing, multi-sensor fusion, and Bayesian regression	Drag coefficients and gust response factors	Questions universal use of code coefficients; the present sensitivity analysis retains the original coefficients and is therefore a screening exercise.

Kenéz and Joó (2024)	Performance-based wind engineering, site monitoring, Bayesian extreme-wind model, and probabilistic FE analysis	Telecommunication lattice mast reliability	Represents uncertainty explicitly; the present study is deterministic but covers a broader superstructure-to-foundation load path.
Zhu et al. (2024)	Nonlinear buckling, incremental dynamic analysis, fragility, and wind directionality	Transmission-tower damage and collapse probability	Shows that oblique attack angles can govern; the present x–y comparison does not constitute a full directional envelope.
Cahyono et al. (2024); Marsia and Siregar (2024)	Code-based BTS upper-structure, connection, and equipment-load assessment	Indonesian BTS tower cases	Direct local comparison; the present study extends the assessment to bored-pile compression, uplift, and flooding.
Calotescu et al. (2025)	Full-scale wind, acceleration, strain, temperature, and video monitoring	50 m telecommunication tower under synoptic and thunderstorm winds	Demonstrates event-type-dependent response; such non-synoptic effects are not represented in the present equivalent-static model.
Moussavi et al. (2025)	Homogenized analytical dynamics and random-vibration analysis	Effect of tapering on telecommunication-tower response	Shows geometry-dependent dynamics; the present study evaluates only one taper and bracing configuration.
Romero Romero et al. (2025)	Comparative SAP2000/STAAD.Pro modal and LRFD assessment	36 m self-supporting telecommunications tower	Identifies secondary-member slenderness despite acceptable global response; supports member-level verification beyond overall stability.
Mengistu et al. (2026)	Two-year full-scale operational modal analysis	Environmental variability and aerodynamic damping of a 50 m lattice tower	Shows that modal properties and damping are not constant; the present model uses fixed analytical properties.
Fahim et al. (2026)	Case implementation of steel construction in a resource-constrained seismic region	Fabrication, logistics, economy, and local implementation	Contextual rather than tower-specific; supports consideration of constructability alongside calculated structural capacity.

The 2023–2026 literature reveals a clear hierarchy of analytical sophistication. At one end, aeroelastic and inverse-identification studies reconstruct dynamic wind forces and reassess aerodynamic coefficients (Zhang et al., 2023a; Zhang et al., 2023b; Jeddi et al., 2023). Performance-based and fragility studies explicitly propagate uncertainty and directionality into failure metrics (Kenéz and Joó, 2024; Zhu et al., 2024). Full-scale monitoring then provides empirical evidence on thunderstorm response, temperature-dependent modal properties, and aerodynamic damping (Calotescu et al., 2025; Mengistu et al., 2026). These approaches provide stronger hazard and response characterization than the deterministic method used here, but they generally require monitoring records, wind-tunnel data, stochastic models, or specialist calibration.

The present study occupies a different methodological tier. Its strength is breadth across the structural load path: wind demand, compression members, bolts, base plate, anchor bolts, pedestal transfer, bored-pile compression, uplift, and flood-adjusted stability are evaluated within one traceable project framework. Its weakness is depth in hazard representation: only equivalent-static wind and principal-axis demand are analysed, uncertainty is not propagated, and the sensitivity scenarios are not complete structural reruns. The comparison therefore does not support a claim that the current method is superior to recent performance-based or monitoring approaches. Instead, it identifies the method as a practical screening and design-verification framework for projects where detailed aerodynamic and probabilistic data are unavailable.

Accordingly, the originality of the paper is an integrated application contribution rather than a new computational theory. The result is useful because it exposes possible inconsistency between subsystem margins: the critical steel-member utilization is relatively low, whereas the flood-adjusted foundation compression reserve is more limited. Such subsystem comparison would be obscured in an upper-structure-only report. The paper also establishes an explicit decision boundary: a change in wind region, antenna configuration, tower geometry, or soil condition requires a new structural analysis rather than proportional transfer of the present safety conclusion.

Limitations and future research

This study is a single-case evaluation and its findings cannot be generalized directly to towers with different height, taper, bracing pattern, base width, steel grade, equipment configuration, wind exposure, seismicity, or soil profile. The sensitivity study scales equivalent wind demand but does not replace complete structural reanalysis for Scenarios S2 and S3. Only the x and y principal directions were examined; oblique wind, thunderstorm/downburst loading, and aeroelastic interference from antennas were not modelled. The analytical model also adopts fixed structural properties and therefore does not capture the temperature-dependent modal variation and wind-dependent damping observed in long-term monitoring studies (Calotescu et al., 2025; Mengistu et al., 2026). Connection slip, fabrication tolerances, corrosion, fatigue, nonlinear soil–pile interaction, liquefaction, scour, and field-measured modal properties were outside the available dataset. Future research should compare three- and four-legged configurations, vary bracing and antenna area, conduct nonlinear buckling and probabilistic fragility analyses, evaluate oblique and non-synoptic winds, and validate the numerical model using full-scale vibration, strain, and wind measurements.

CONCLUSION

1. The y-direction equivalent wind load was 56.69 kN, 15.46% larger than the x-direction load of 49.10 kN; consequently, COMB4 governed the reported structural checks.

2. The critical L150×150×15 leg member carried 287.50 kN against a design compressive resistance of 652.71 kN, giving a utilization ratio of 0.44. All reported compression-member ratios were below the project threshold of 0.95.

3. The evaluated bolt group, base plate, and anchor-bolt system satisfied the applied factored demands, maintaining a continuous design load path from the tower leg into the concrete pedestal.

4. The bored-pile system satisfied both direct and flood-adjusted checks. Under the flood-adjusted condition, compression resistance was 422.44 kN against 376.81 kN demand, and uplift resistance was 341.17 kN against 267.76 kN demand.

5. The wind-speed sensitivity assessment showed that equivalent wind demand increased by factors of 1.88 and 3.049 when the basic wind speed increased from 33.33 m/s to 45.70 and 58.20 m/s. Therefore, the adequacy conclusion is valid only for the modeled geometry, materials, equipment, site coefficients, CPT data, and load combinations; it should not be transferred to another tower or wind region without complete reanalysis.

ACKNOWLEDGMENTS

The authors gratefully acknowledge PT Hutama Karya (Persero) for providing the project data used in this study.

Conflict Of Interest

The authors declare that they have no conflict of interest related to this study.

Data Availability

The project drawings, calculation sheets, SAP2000 model, and site investigation data contain project-specific information and are available from the corresponding author subject to permission from the data owner.

Author Contributions

D.P.R.: conceptualization, structural analysis, data curation, and original draft. A.Sa.: methodology and design-code review. A.Su.S.: verification and technical interpretation. N.Y.: supervision, review, and editing. All authors reviewed and approved the final manuscript.

REFERENCES

1. Badan Standardisasi Nasional (2019) SNI 1726:2019: Tata cara perencanaan ketahanan gempa untuk struktur bangunan gedung dan nongedung. Jakarta: Badan Standardisasi Nasional.
2. Badan Standardisasi Nasional (2020a) SNI 1727:2020: Beban desain minimum dan kriteria terkait untuk bangunan gedung dan struktur lain. Jakarta: Badan Standardisasi Nasional.
3. Badan Standardisasi Nasional (2020b) SNI 1729:2020: Spesifikasi untuk bangunan gedung baja struktural. Jakarta: Badan Standardisasi Nasional.
4. Cahyono, H.S., Mulyono, J., Carina, A., Wicaksono, M.H. and Waluyo, M.K.H. (2024) ‘Upper-structure analysis of BTS tower on high wind speed area’, DEARSIP: Journal of Architecture and Civil, 4(2), pp. 119–133. doi: 10.52166/dearsip.v4i02.7800.
5. Calotescu, I., Bîtcă, D. and Repetto, M.P. (2025) ‘Full-scale monitoring of a telecommunication lattice tower under synoptic and thunderstorm winds’, Journal of Wind Engineering and Industrial Aerodynamics, 258, 106022. doi: 10.1016/j.jweia.2025.106022.
6. Fahim, A.S., Azizi, H. and Rasa, A.Y. (2026) ‘Pioneering light-gauge steel construction in Afghanistan: A case study of pilot initiatives in Badakhshan Province’, Sigma Journal of Engineering and Natural Sciences, 44(3). doi: 10.14744/sigma.2026.1961.
7. Hardiyatmo, H.C. (2018) Analisis dan perancangan fondasi I. 3rd edn. Yogyakarta: Gadjah Mada University Press.
8. Jeddi, A.B., Azzi, Z., Shafieezadeh, A., Elawady, A., Gan Chowdhury, A. and Irwin, P. (2023) ‘Revisit of underestimated wind drag coefficients and gust response factors of lattice transmission towers based on aeroelastic wind tunnel testing and multi-sensor data fusion’, Engineering Structures, 278, 115486. doi: 10.1016/j.engstruct.2022.115486.
9. Kenéz, Á. and Joó, A.L. (2024) ‘Performance-based wind engineering assessment of a telecommunication mast utilizing Bayesian extreme wind velocity model’, Stochastic Environmental Research and Risk Assessment, 38, pp. 727–749. doi: 10.1007/s00477-023-02596-w.
10. Marsia, N.S. and Siregar, C.A. (2024) ‘Studi kekuatan menara BTS (Base Transceiver Station) pada menara SST tinggi 72 m tipe greenfield’, Sistem Infrastruktur Teknik Sipil, 4(2), pp. 266–284. doi: 10.32897/simteks.v4i2.3950.
11. Mazaheri, P. and Alipour, A. (2026) ‘Investigation of transmission tower system performance under wind directionality effects using large-scale aeroelastic testing’, Journal of Structural Engineering, 152(1), 04025240. doi: 10.1061/JSENDH.STENG-15035.
12. Mengistu, M.T., Maes, K., Calotescu, I., Lombaert, G. and Repetto, M.P. (2026) ‘Experimental assessment of the long-term variation of modal properties and aerodynamic damping of a self-supporting lattice tower’, Journal of Wind Engineering and Industrial Aerodynamics, 273, 106436. doi: 10.1016/j.jweia.2026.106436.
13. Meyerhof, G.G. (1976) ‘Bearing capacity and settlement of pile foundations’, Journal of the Geotechnical Engineering Division, ASCE, 102(GT3), pp. 195–228.

14. Moussavi, S.H., Khodaygan, S. and Durali, M. (2025) ‘The effect of tapering angle on structural dynamics of pseudo-periodic structures: Application to wind induced vibrations of telecommunication towers’, Mechanics Based Design of Structures and Machines, 53(7), pp. 5341–5359. doi: 10.1080/15397734.2025.2464759.
15. Romero Romero, C.A., Quinde Rangel, R.L. and Fritzner, J. (2025) ‘Análisis comparativo revisión estructural de una torre metálica autosoportada de 36 metros de altura para uso de telecomunicaciones’, Impacto Científico, 20(2), pp. 396–418. doi: 10.5281/zenodo.18175320.
16. Saleem, S., Hejazi, F. and Ostovar, N. (2023) ‘Health monitoring of ultra high fiber performance reinforced concrete communication tower using machine learning algorithms’, Journal of Civil Structural Health Monitoring, 13, pp. 1105–1130. doi: 10.1007/s13349-023-00688-3.
17. Zhang, W., Li, C., Liu, G. and Xiao, Y. (2023a) ‘Estimation of dynamic wind forces on a steel lattice tower based on generalized wind force spectra’, Structures, 48, pp. 1634–1650. doi: 10.1016/j.istruc.2022.12.073.
18. Zhang, W., Li, C., Liu, G. and Xiao, Y. (2023b) ‘Reconstruction of dynamic wind forces on a transmission steel lattice tower using aeroelastic wind tunnel test data’, Engineering Structures, 275, 115167. doi: 10.1016/j.engstruct.2022.115167.
19. Zhu, C., Yang, Q., Huang, G., Zhang, X. and Wang, D. (2024) ‘Fragility analysis and wind directionality-based failure probability evaluation of transmission tower under strong winds’, Journal of Wind Engineering and Industrial Aerodynamics, 246, 105668. doi: 10.1016/j.jweia.2024.105668.